ESTIMATION OF RADIOMETRIC UNCERTAINTY AFTER SMILE CORRECTION

Karim Lenhard[1] **and Andreas Baumgartner**[2]

[1]*German Aerospace Research Center, Remote Sensing Technology Institute, Muenchener Str. 20, 82234 Wessling, Germany, Email: karim.lenhard@dlr.de*

[2]*German Aerospace Research Center, Remote Sensing Technology Institute, Muenchener Str. 20, 82234 Wessling, Germany, Email: andreas.baumgartner@dlr.de*

ABSTRACT

With the increasing use of hyperspectral remote sensing, the importance of the determination of the measurement uncertainties for spectral radiance data has been recognized. Analytical error propagation can not be used for estimating the influence of complex instrument properties such as smile or stray light, and their respective correction algorithm. A Monte Carlo analysis using a simplified model sensor similar to the imaging spectrometer ROSIS and synthetic data is performed in order to analyze the uncertainty for a smile correction resampling algorithm.

Key words: Measurement uncertainty; Monte Carlo Analysis; Smile effect; Spectral calibration; Radiometric calibration.

1. INTRODUCTION

The measurement uncertainties of individual parameters of imaging spectrometers, e.g. radiometric response, center wavelength or bandwidth of individual spectral channels, might be known through laboratory calibration. Yet, the resulting measurement uncertainty of the measured data cannot be derived easily from those numbers - E.g. [4] demonstrated that in the case of large gradients occurring in recorded spectra, even small uncertainties ($\approx$ 5 %) of the center wavelength of a spectral channel can result in radiometric errors in the order of 10 %. For an estimation of this effect for DLRs imaging spectrometer ROSIS [2] due to the sensors inherent smile effect, see fig. 1. The plot has been calculated with a reflectance spectrum of grass for a spectral shift of $\Delta\lambda = 1.2\,\mathrm{nm}$. The large errors in the corrected spectrum up to channel 10 are due to noise in the radiometric response curve of ROSIS.

In order to mitigate such errors, it is necessary to perform individual spectral calibration of each geometric pixel. However, the end-users expect a "uniform" product [8], i.e. the center wavelengths of the spectrometer channels should be constant across the field of view. To solve this contradiction, a resampling of the measured spectra to a set of reference wavelengths is required.

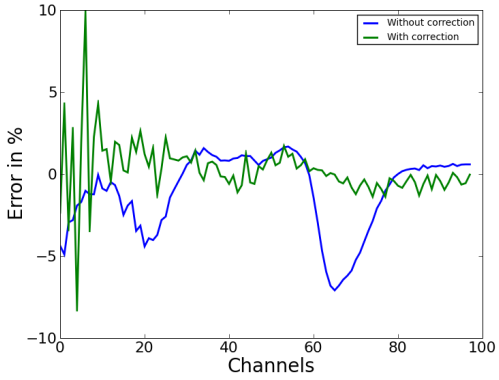

Figure 1. Blue: Radiometric errors due solely to spectral misregistration. Green: Remaining error after correction.

According to metrological guidelines [6], propagation of measurement uncertainties should be performed numerically with a Monte Carlo analysis (MCA) if an analytical solution is not readily available. Both the radiometric uncertainty due to spectral uncertainty as well as the residual radiometric uncertainty after correction for spectral smile can not be estimated analytically. Consequently such a MCA will be described below, as well for smile-corrected data, as for non-corrected data, in order to allow a comparison. As airborne or laboratory data can not be used for a MCA, synthetic data has to be generated for the analysis.

2. THE SIMULATED INSTRUMENT

For the MCA, the simulated instrument was chosen to be similar to the airborne instrument ROSIS. The chosen characteristics of this model sensor are shown in table 1.

An actual radiometric response function of ROSIS was

Table 1. Properties of the simulated instrument

Wavelength range	430 nm - 830 nm
Spectral channels	100
Spectral sampling interval	4 nm
Spectral response function	Gaussian, FWHM = 6 nm
Number of geometric pixels	512

Table 2. Assumed measurement uncertainties for the MCA

Radiometric uncertainty of calibration standard	± 2 %
Spectral uncertainty of center wavelengths	$\pm$ 0.2 nm / $\pm$ 0.6 nm with/without smile correction
Noise	$3.5 \cdot 10^{-4} \cdot$ max. signal
Spectral uncertainty of smile shift	± 0.1 nm

used to convert the simulated radiances into a value proportional to digital numbers (DN).

The measurement uncertainties are assumed as having a Gaussian distribution. The values listed in table 2 correspond to the widths (1 σ) of those distributions.

2.1. The smile effect in ROSIS

The parameters of the smile effect are derived from actual measurement data of ROSIS. As proposed in [5], the center wavelengths are retrieved from the spectral position of an atmospheric feature in not-atmospherically corrected data.

To measure the spectral smile, the position of the absorption feature of atmospheric O_2 at 762 nm with respect to the spectral channels of each geometric pixel of the instrument is calculated.

This is done by using a regular, earth-looking in-flight measurement with ROSIS. All hyperspectral frames of this data set are averaged to reduce the influence of the varying ground spectra. To each of the 512 spectra obtained, a Gaussian function is fitted to the oxygen absorption dip. From each fit, the center of the Gaussian function is recorded. Fig. 2 shows the determined center positions of the absorption dip as well as a second order polynomial fit. The polynomial function is used subsequently for the calculation of the center wavelengths of all spectral channels. The total shift in center wavelengths amounts to 0.3 channels, which corresponds to $\Delta\lambda = 1.2\,\mathrm{nm}$.

In general, spectral smile can have a dependency on spectral channels. As such knowledge is not yet available for ROSIS, the spectral shifts due to the smile effect are assumed constant over all channels. Future measurements of the smile of ROSIS for several wavelengths are planned in DLRs calibration laboratory for imaging spectrometers [3].

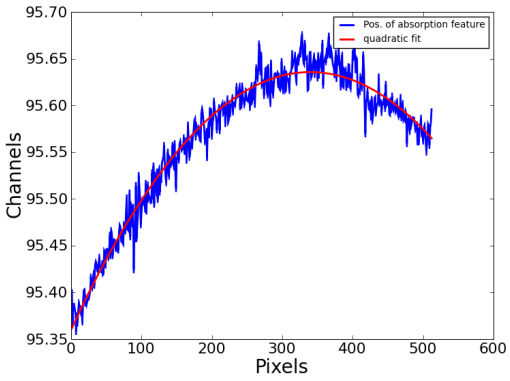

Figure 2. Measured position of atmospheric absorption feature on detector and parabolic fit to the data

3. MONTE CARLO ANALYSIS

The Monte Carlo analysis for the propagation of uncertainties is done by generating frames from sample spectra (e.g. grass, corn, water, etc.), adding statistically distributed measurement errors, introducing systematic shifts in center wavelengths corresponding to the smile, correcting the smile, and saving them to allow further analyses. As the entire frame generation process is synthetic, "true" reference spectra can be calculated for comparison.

3.1. Number of samples

According to [6], the number of calculated frames should be high enough to be statistically significant, yet as low as possible to minimize computing time. As no method of determining beforehand an exact number of required Monte Carlo iterations exists, a number of 200 frames for each sample spectrum was chosen for this study. As 20 sample spectra are used, a total of 4000 frames is calculated.

3.2. Generation of synthetic hyperspectral data

Each frame corresponds to 512 spectra of an uniformly illuminated, uniform surface with an uniform atmosphere between the sensor and the scene. For each spectrum, new random numbers are generated from the distributions given in table 2. In the equations below, i denotes the

spectral channel number, while j indexes the geometric pixels.

The generation of a hyperspectral frame that includes measurement uncertainties is realized as follows:

1. An at-sensor reflectance S is calculated as follows:

$$S(\lambda) = \text{refl}(\lambda) \cdot \text{atmo}(\lambda) \cdot \text{sun}(\lambda) \quad . \tag{1}$$

   In this equation, $\text{refl}(\lambda)$ denotes the sample reflectance spectrum, $\text{atmo}(\lambda)$ an atmospheric transmission spectrum generated with MODTRAN [1] and $\text{sun}(\lambda)$ [7] a solar irradiance spectrum. All spectra have a higher resolution ($\Delta\lambda \approx 1\,\text{nm}$) than the simulated instrument.

2. The center wavelength of each spectral channel is calculated according to the smile polynomial defined in sec. 2.1 and varied in the range of the uncertainty.

3. For each geometric pixel, the spectrum is sampled by integrating the product of the spectral response function $\text{SRF}(\lambda)$ of each channel with the spectrum:

$$DN'_{i,j} = \int \text{SRF}(\lambda)_{i,j} \cdot S(\lambda) d\lambda \quad . \tag{2}$$

   $DN_{i,j}$ corresponds to the signal of a single synthetic detector element.

4. The frame is multiplied with the actual radiometric response function $\text{resp}(i)$ of ROSIS:

$$DN_{i,j} = DN'_{i,j} \cdot \text{resp}(i) \quad . \tag{3}$$

5. The signal of each virtual detector element is varied within the range of the radiometric uncertainty.

6. Noise is added to the signal of each detector element.

7. The frame is corrected for smile by resampling each spectrum to a set of defined reference wavelengths.

Additionally, another set of 4000 frames is generated. For this second set, the center wavelengths of the spectral channels are assumed constant over all geometric pixels. This corresponds to the case where the smile of an instrument has not been determined. To reflect this, the uncertainty of the spectral calibration is increased to $\pm 0.6\,\text{nm}$.

4. RESULTS

In the following, some results are presented. The plots in this section are presented as histograms of the distributions of the normalized deviations of a single detector element from the reference detector element. The normalized deviation is defined as follows:

$$\text{Normalized Deviation}_{i,j} = \frac{DN_{i,j} - DN_{\text{ref}}}{DN_{\text{ref}}} \cdot 100\% \quad . \tag{4}$$

DN_{ref} corresponds to the "true" signal level of the calculated reference. A first result is that the distribution of the values resulting from the MCA is in general not Gaussian. This is illustrated in fig. 3: large deviations of 10 % or more from the reference spectrum occur more often as the fitted Gaussian distribution could account for.

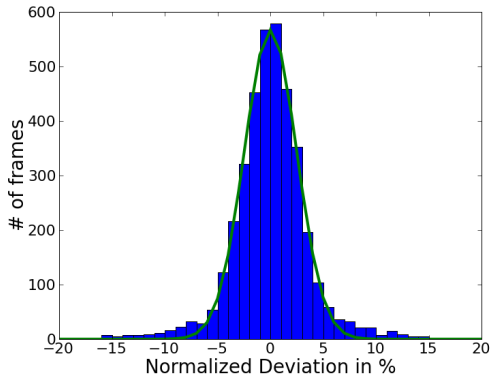

Figure 3. Comparison of the resulting distribution of the MCA with a fitted Gaussian function

Also, the assumption that that detector elements with lower signal levels have larger uncertainties as those with higher signal level can be easily verified (see fig. 4). As the resulting distribution is not Gaussian, the measurement uncertainties can not be specified in units of width, or σ, of a Gaussian function. The criterion chosen to indicate errors in this case is that 95 % of all histogram entries have to be between the indicated boundaries.The signal levels are $DN_{\text{high}} \approx 0.4 \cdot DN_{\text{max}}$ and $DN_{\text{low}} \approx 0.1 \cdot DN_{\text{max}}$. For the depicted detector ele-

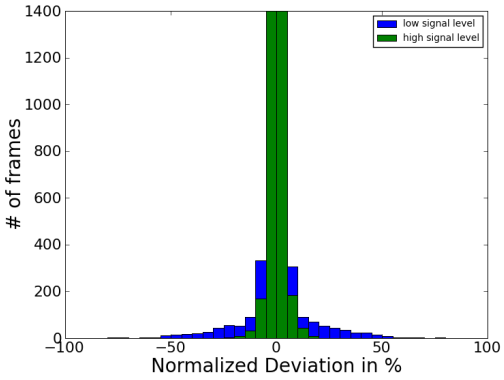

Figure 4. Comparison between detector elements with high and low signal levels

ments, this means:

$$\Delta DN_{\text{high}} \approx \pm 8\% \quad (5)$$

$$\Delta DN_{\text{low}} \approx \pm 30\% \quad (6)$$

It should be noted that even for the detector element with high signal level, the total radiometric uncertainty is twice as high as just the radiometric uncertainty of the calibration standard.

Fig. 5 compares the uncertainties for one detector element, with and without smile correction. The two histograms are created from 200 frames generated from a single spectrum, and are given for the detector element that suffers most from the smile effect (channel 65 in fig. 1) - This is a worst case scenario. Although exact

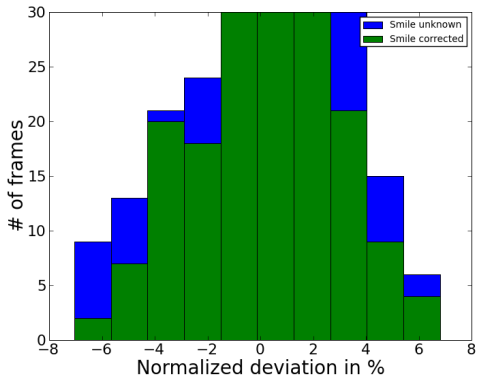

Figure 5. Comparison between smile corrected data and data for which smile is not known (for a large error due to spectral uncertainty)

values for the uncertainties can not be given with this few histogram entries, fig. 5 shows that the uncertainty is clearly reduced by the correction algorithm - which is concordant with fig. 1.

In contrast, the uncertainties of a detector element, where the center wavelength does not differ from the reference wavelength for this channel, the signal distributions resulting from the MCA are similar. Such histograms can show that a correction through resampling does not deteriorate the radiometric uncertainty. This is shown in fig. 6

5. CONCLUSION

This simulation shows how to propagate spectral uncertainties according to [6]. Also, Monte Carlo analyses can quantify the benefit of correction techniques, exemplified here with the smile correction, and calculate their contribution to the uncertainty budget.

Additionally, it has been illustrated, that spectral resampling can reduce the total radiometric measurement uncertainty when large gradients occur in the measured

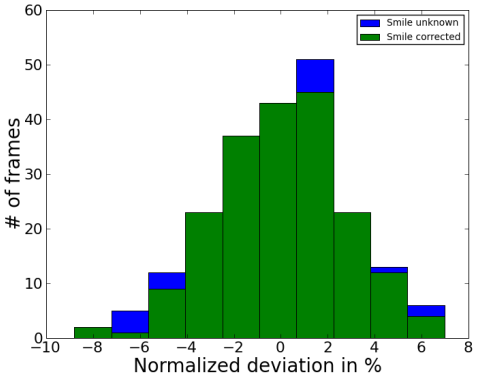

Figure 6. Comparison between smile corrected data and data for which smile is not known (for a small error due to spectral uncertainty)

spectra, but does not affect significantly the uncertainty at wavelengths, where such gradients do not occur.

For this kind of MCA to lead to valuable results, an entire level 1 processing algorithm will need to be analyzed this way, with exact laboratory inputs on the measurement uncertainties of the individual parameters of the respective sensor. This is planned for the near future. It will provide reliable measurement uncertainties for imaging spectrometer data.

REFERENCES

1. A Berk, L.S. Bernstein, and D.C. Robertson. Modtran: A moderate resolution model for lowtran 7. Technical report, Geophysics Laboratory, Air Force Command, U.S. Air Force, Hanscom, AFB, MA, USA, 1989.

2. P. Gege, D. Beran, W. Mooshuber, J. Schulz, and H van der Piepen. System analysis and performance of the new version of the imaging spectrometer rosis. *Proc. 1st EARSeL Workshop on Imaging Spectroscopy*, 1:29–35, October 1998.

3. Peter Gege, Jochen Fries, Peter Haschberger, Paul Schoetz, Horst Schwarzer, Peter Strobl, Birgit Suhr, Gerd Ulbrich, and Willem Jan Vreeling. Calibration facility for airborne imaging spectrometers. *ISPRS Journal of Photogrammetry and Remote Sensing*, 64(4):387–397, JUL 2009.

4. R. O. Green. Spectral calibration requirement for earth-looking imaging spectrometers in the solar-reflected spectrum. *Applied Optics*, 37(4):683–690, 1998. Cited By (since 1996): 44.

5. L. Guanter, R. Richter, and J. Moreno. Spectral calibration of hyperspectral imagery using atmospheric absorption features. *Applied Optics*, 45(10):2360–2370, 2006. Cited By (since 1996): 11.

6. JCGM, editor. *Evaluation of measurement data - Supplement 1 to the "Guide to the expression of uncertainty in measurement" - Propagation of distributions using a Monte Carlo Method*. 2008.

7. H. Neckel and D Labs. The solar radiation between 3300 and 12500 . *Sol. Phys.*, 90:205–258, 1984.

8. J. Nieke, D. Schlapfer, F. Dell'Endice, J. Brazile, and K.I. Itten. Uniformity of imaging spectrometry data products. *Geoscience and Remote Sensing, IEEE Transactions on*, 46(10):3326 –3336, oct. 2008.